

# Superconductivity in layered Zintl phase $\text{LiSn}_2\text{As}_2$

Junjie Wang<sup>†,1,2</sup> Xiangru Cui<sup>†,1,2</sup> Yimin Wan<sup>†,3</sup> Tianping Ying<sup>\*,1</sup> Shiyao Li<sup>3</sup> and Jiangang Guo<sup>\*,1,2,4</sup>

<sup>1</sup>*Beijing National Laboratory for Condensed Matter Physics,  
Institute of Physics, Chinese Academy of Sciences, Beijing 100190, China*

<sup>2</sup>*School of Physical Sciences, University of Chinese Academy of Sciences, Beijing 100049, China*

<sup>3</sup>*State Key Laboratory of Surface Physics, Department of Physics, Fudan University, Shanghai 200438, China*

<sup>4</sup>*Songshan Lake Materials Laboratory, Dongguan 523808, China*

(Dated: November 23, 2021)

We report the superconductivity in the layered Zintl phase  $\text{LiSn}_2\text{As}_2$ , which is isostructural to  $\text{NaSn}_2\text{As}_2$  and has a transition temperature ( $T_c$ ) of 1.6 K. Despite similar  $T_c$  and Debye temperatures, substituting of Na with Li considerably increases the upper critical field. Based on a systematically comparison of  $\text{Sn}_4\text{As}_3$ ,  $\text{NaSnAs}$ ,  $\text{NaSn}_2\text{As}_2$ ,  $\text{Na}_{1-x}\text{Sn}_2\text{P}_2$ ,  $\text{SrSn}_2\text{As}_2$ , and  $\text{LiSn}_2\text{As}_2$ , we propose that carrier doping, intimately related to the formation of lone-pair electrons, controls superconductivity in layered SnAs-based compounds rather than chemical pressure. The current findings provide a thorough and comprehensive understanding of Sn-based Zintl phase.

## I. INTRODUCTION

The Zintl phase is the product where alkali metal or alkaline earth reacts with any post-transition metals (Group 13 or 14) or  $p$  elements [1, 2]. There is usually a complete electron transfer from the more electropositive metal to anion clusters (Zintl ion), such as  $(\text{Si}_4)^{4-}$  [3],  $(\text{Tl}_4)^{8-}$  [4] and  $(\text{As}_7)^{3-}$  [5]. When the Zintl ion is composed of infinite 2D layers, these compounds are called layered Zintl phase with numerous features including superconductivity [6, 7], topological properties [8–11] and thermoelectricity [12, 13].  $\text{NaSn}_2\text{As}_2$ , with a superconducting transition temperature at 1.6 K, has recently attracted a lot of attention [6, 14]. Later research discovered that  $\text{NaSn}_2\text{As}_2$  can be prepared into few layers by mechanical and liquid-phase exfoliation. Substitution of As for a smaller P will increase the  $T_c$  to 2 K [7], while  $\text{SrSn}_2\text{As}_2$  is proved to be a 3D Dirac semimetal without superconductivity [15, 16]. Detailed investigation suggests the  $T_c$  enhancement in  $\text{Na}_{1-x}\text{Sn}_2\text{P}_2$  is due to additional charge donation from Na vacancies. However, the positive chemical pressure generated by P with a small radius can not be neglected. By the same token, replacing Na with a greater Sr will result in a negative pressure, which is consistent with the absence of superconductivity in  $\text{SrSn}_2\text{As}_2$ . As a result, the increase in  $T_c$  in the SnAs-based layered Zintl phase cannot be attributed solely to carrier doping or chemical pressure.

$\text{NaSnAs}$  and  $\text{NaSnP}$  [17, 18], on the other hand, are two closely  $\text{NaSn}_2\text{As}(\text{P})_2$  related compound by inserting one more Na ion in each  $\text{SnAs}(\text{P})$  layer (Fig. 1(b)). Different from  $\text{NaSn}_2\text{As}_2$  and  $\text{Na}_{1-x}\text{Sn}_2\text{P}_2$  [7, 14],  $\text{NaSnAs}$  and  $\text{NaSnP}$  are indirect band gap semiconductors with narrow gaps of about 0.31 and 0.62 eV, respectively [12]. It is reported that  $\text{NaSnAs}(\text{P})$  shows a much lower thermal conductivities than  $\text{NaSn}_2\text{As}(\text{P})_2$  due to the surplus lone-pair electrons. The lone pair is defined as a pair of valence electrons that are not shared with another atom to form a covalent bond. Sn and As(P) are covalently

bonded to form a tetrahedron, as shown in Fig. 1(e). In the case of  $\text{NaSnAs}(\text{P})$ , with the one electron from Na, both Sn and As(P) enter a full outer shell structure, leaving two sets of lone-pair electrons dangling outside of the plane.  $\text{SrSn}_2\text{As}_2$  follows the same logic, as Sr contributes two electrons to the system. Previous research found that surplus lone-pair electrons will generate strong in-harmonic vibration and increase the Gruneisen parameters [19–21]. To fully understand the dominant factor of superconductivity in the series of Sn-based layered Zintl phase, new compounds that may generate chemical pressure without introducing extra carrier doping are highly desired.

In this work, we report the discovery of a new compound  $\text{LiSn}_2\text{As}_2$  that is isostructural to  $\text{NaSn}_2\text{As}_2$ . Compared with  $\text{NaSn}_2\text{As}_2$ ,  $\text{LiSn}_2\text{As}_2$  has a similar  $T_c$  at 1.6 K, but a much-enhanced upper critical field ( $H_c$ ). First principle calculation reveals a significant change of the Fermi surface topology by the substitution of Li. Combined with experimental and theoretical analyses, we infer that the appearance of superconductivity in A-Sn-As system is dominated by the charge carrier doping, rather than chemical pressure. Finally, we provide a unified understanding towards the reported Sn-based layered Zintl phases, with  $\text{NaSn}_2\text{Pn}_2$  serving as a parent phase for the series of superconductors.

## II. EXPERIMENTS

### Synthesis

Stoichiometric amount of Li, Sn, and As were mixed and loaded into an alumina crucible, sealed into an evacuated quartz tube. Heated to 925 K with duration of 20 hours. Then, the sintered sample was taken out, reground, pelletized and heated to 900 K for 20 hours for adequate distribution. The sample preparation process are handled in a glove-box filled with argon gas.  $\text{LiSn}_2\text{As}_2$  single crystals can be grown by using Sn-flux

method, the sealed quartz tube was heated to 1200 K in 20 hours, slowly cooled to 1000 K with a rate of 3 K/h. The excess Sn is removed by centrifugation. Single crystal with size of  $1.5 \times 1.5 \times 0.1 \text{ mm}^3$  can thus be obtained.

### Characterization

Powder X-ray diffraction (XRD) data were collected using a PANalytical X'Pert PRO diffractometer (Cu  $K\alpha$ -radiation) with a graphite monochromator in a reflection mode. Rietveld refinement of PXRD pattern was performed using Fullprof software suites [22]. The composition of Sn and As was determined by Energy Dispersive Spectroscopy (EDS), the elements ratio and element valence state information of Li, Sn and As were determined by inductively coupled plasma atomic emission spectroscopy and X-ray photoelectron spectroscopy (ICP-AES and XPS). Electrical resistivity and Hall resistivity were measured through standard six-wire method using the physical property measurement system (PPMS-9T, Quantum Design).

### Theoretical calculation

First-principles calculations were carried out with the density functional theory (DFT) implemented in the Vienna ab initio simulation package (VASP) [23]. The generalized gradient approximation (GGA) in the form of Perdew-Burke-Ernzerhof (PBE) [24] was adopted for the exchange-correlation potentials. We used the projector augmented-wave (PAW) [25] pseudopotentials with a plane wave energy of 800 eV;  $1s^22s^1$ ,  $4d^{10}5s^25p^2$  and  $4s^24p^3$  were treated as valence electrons for Li, Sn and As, respectively. A Monkhorst-Pack Brillouin zone sampling grid with a resolution  $0.02 \times 2\pi \text{ \AA}^{-1}$  was applied [26]. Atomic positions and lattice parameters were fully relaxed till all the forces on the ions were less than  $10^{-4} \text{ eV/\AA}$ . The lattice parameters after relaxation were  $a = 4.03085 \text{ \AA}$  and  $c = 25.85439 \text{ \AA}$ , agreeing well with the experimental values within a deviation of 0.6%. This confirmed the reliability of the calculation. Phonon spectra were calculated on a  $2 \times 2 \times 1$  supercell using the finite displacement method implemented in the PHONOPY code to determine the lattice dynamical stability of the structures [27]. The band structure of  $\text{NaSn}_2\text{As}_2$  was calculated for comparison using the same parameter except for the cut off energy was set to be 400 eV.

## III. RESULTS AND DISCUSSION

$\text{LiSn}_2\text{As}_2$  is a new compound, isostructural to the well-studied  $\text{NaSn}_2\text{As}_2$ . Figure 1 depicts all of the known Sn-based Zintl phase, including  $\text{Sn}_4\text{As}_3$ ,  $\text{NaSnAs}$  and  $\text{ASn}_2\text{Pn}_2$  ( $A = \text{Li/Na/Sr}$ ,  $\text{Pn} = \text{As/P}$ ), which crystallize in a space group of  $R\bar{3}m$  (No.166) and can be viewed as different stacking sequence of the SnPn layers with Na or other guest species. As shown in Fig. 1(a),  $\text{Sn}_4\text{As}_3$  has two types of Sn-As configurations [28]. In one build-

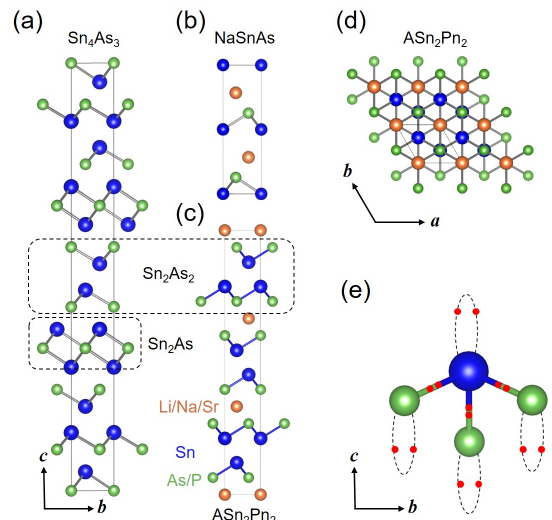


FIG. 1. (a-c) Crystal structures of  $\text{Sn}_4\text{As}_3$ ,  $\text{NaSnP}$ ,  $\text{ASn}_2\text{Pn}_2$  ( $A = \text{Li/Na/Sr}$ ,  $\text{Pn} = \text{As/P}$ ). (d) The crystal structure of  $\text{ASn}_2\text{Pn}_2$  along the  $c$ -direction. (e) Schematic diagram of long-pair electrons in Sn-based compound systems.

ing block, each Sn (As) atom is coordinated by three As (Sn) atom to form a  $\text{Sn}_2\text{As}_2$  layer, while the other Sn atom is joined to six As atoms to form a  $\text{Sn}_2\text{As}$  layer. As a result,  $\text{Sn}_4\text{As}_3$  can be written as  $(\text{Sn}_2\text{As})\text{Sn}_2\text{As}_2$  (Fig. 1(a)),  $\text{NaSnAs}$  (Fig. 1(b)) and  $\text{NaSn}_2\text{Pn}_2$  (Figs. 1(c) and (d)) share a similar stacking sequence of SnPn and A layers with the variation of Na in each SnPn layer or every two layers along the  $c$  axis. Figure 1(e) is the schematic diagram of the local electronic configuration of the SnAs tetrahedra. The covalent bonds between Sn and As are composed of the  $p$  orbitals, while the dangling lone-pair electrons are contributed by the  $s^2$  orbitals of Sn and As. For  $\text{NaSnPn}$  and  $\text{SrSn}_2\text{As}_2$ , the lone-pair orbitals are fully occupied, while the lone-pair on the Sn side is proved to be partially occupied in  $\text{NaSn}_2\text{As}_2$ .

Figure 2(a) shows the Rietveld refinements of powder diffraction pattern of  $\text{LiSn}_2\text{As}_2$ , yielding the lattice constants  $a = 4.0072(3) \text{ \AA}$  and  $c = 25.7008(6) \text{ \AA}$ . The refinement converged to the figures of merit  $R_p = 5.32\%$ ,  $R_{wp} = 7.36\%$  and  $\chi^2 = 2.63$ . The lattice change of the  $a$  and  $c$  axes are  $-0.02\%$  and  $6.82\%$ , respectively, as compared to  $\text{NaSn}_2\text{As}_2$  with  $a = 4.006 \text{ \AA}$ ,  $c = 27.581 \text{ \AA}$  [12], demonstrating the realization of chemical pressure. The diffraction pattern of a single crystal  $\text{LiSn}_2\text{As}_2$  sample with  $00l$  preferred orientation is shown in Fig. 2(b), and the optical image is shown in the inset. XPS and ICP measurements were used to validate the element ratio and valence states in  $\text{LiSn}_2\text{As}_2$ . As the XPS spectra of Li  $1s$  orbital shown in Fig. 2(c), the binding energy of Li  $1s$  is  $54.3 \text{ eV}$ , consisting with that of  $\text{Li}^+$ . This shows that the Li ion has entirely lost its out shell electron to  $(\text{Sn}_2\text{As}_2)^-$ . Besides, the peaks of Sn  $3d^{3/2}$  and

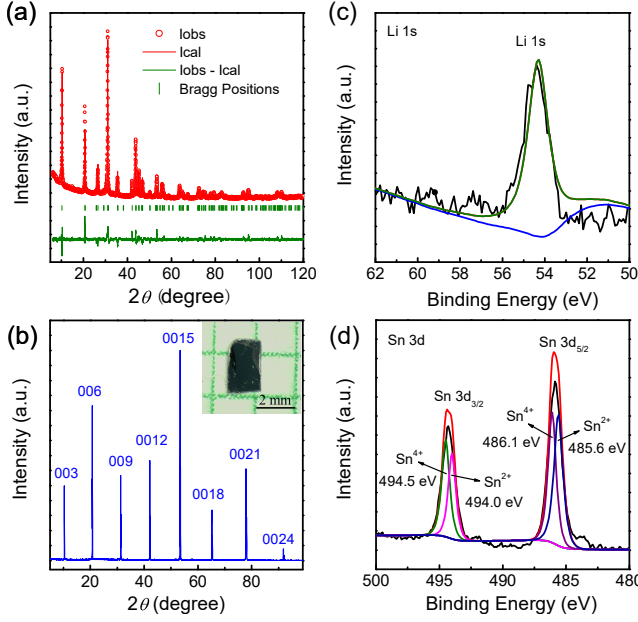


FIG. 2. (a) Rietveld refinements of powder x-ray diffraction (PXRD) pattern of LiSn<sub>2</sub>As<sub>2</sub> at temperature at 300 K. (b) The XRD patterns of LiSn<sub>2</sub>As<sub>2</sub> single crystal, where the preferred orientation of 00*l* peaks can be seen. Inset shows the optical images of LiSn<sub>2</sub>As<sub>2</sub> single crystal. (c, d) XPS spectrum of Li-1*s* Sn-3*d* orbit of LiSn<sub>2</sub>As<sub>2</sub>.

$3d^{5/2}$  orbitals locate at 494.3 eV and 485.9 eV, respectively (Fig. 2(d)), and both of them can be separated into Sn<sup>4+</sup> and Sn<sup>2+</sup> peaks. Meanwhile, the chemical formula of stoichiometric Li:Sn:As = 1:2:2 is determined by ICP. LiSn<sub>2</sub>As<sub>2</sub> single crystal exhibits a metallic behavior from 2 to 300 K (Fig. 3(a)). The residual resistivity ratio (RRR) value is calculated to be 1.36, which is lower than that of NaSn<sub>2</sub>As<sub>2</sub> at 3.7 [14]. To further comprehend its normal state behavior of LiSn<sub>2</sub>As<sub>2</sub>, we use the Bloch-Gruneisen (BG) model to fit the resistance curve [29, 30]

$$\rho(T) = \rho_0 + 4R(\Theta_R) \left( \frac{T}{\Theta_R} \right)^z \int_0^{\frac{\Theta_R}{T}} \frac{x^z dx}{(e^x - 1)(1 - e^{-x})}$$

where  $T$  stands for temperature and  $\Theta_R$  for Debye temperature. For electron-electron interaction,  $s$ - $d$  electron scattering, and electron scattering by phonons, the value  $z$  could be 2, 3, or 5. The fitting curves of three alternative scattering mechanisms are shown in Figure 3(a). The raw data is best fitted by the curve with  $z=5$ . In the LiSn<sub>2</sub>As<sub>2</sub> system, the phonon dominates the scattering of normal state resistance. Other fitting parameters are  $\rho_0=0.499$  mΩ·cm,  $\rho(\Theta_R)=0.614$  mΩ·cm and  $\Theta_R=194$  K. To ensure that the BG fitting is correct, we measured the heat capacity of a single LiSn<sub>2</sub>As<sub>2</sub> crystal, as shown in Fig. 3(b). The dotted line in Fig. 3(b) represents the Dulong-Petit limit, which is closed at  $C_p$  (200 K)=118.64 J mol<sup>-1</sup> K<sup>-1</sup>. The inset shows  $C_p/T$  as a function of  $T^2$

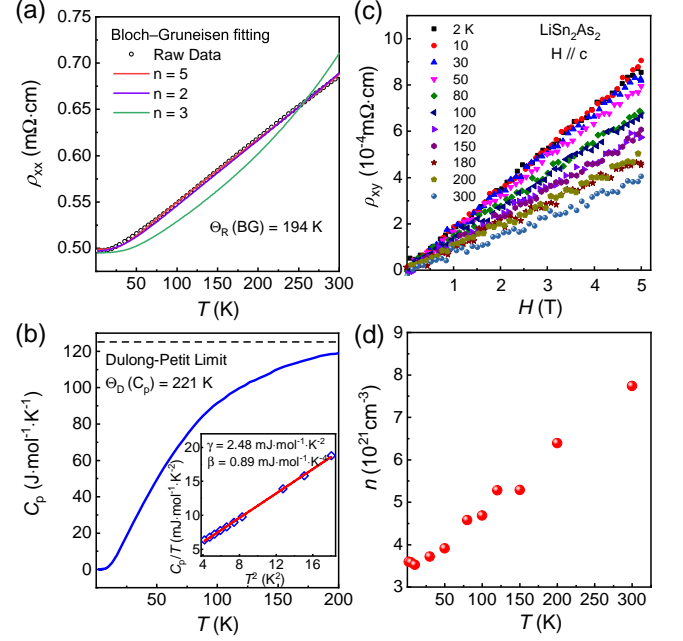


FIG. 3. (a) Resistivity of the LiSn<sub>2</sub>As<sub>2</sub> single crystal from 2 to 300 K, the circles represent raw data and the solid lines are Bloch-Gruneisen fitting curve with  $z=2,3$  and 5. (b) Specific heat ( $C_p$ ) as a function of temperature of LiSn<sub>2</sub>As<sub>2</sub> single crystal. Inset shows  $C_p/T$  as a function of  $T^2$  from 2-5 K. (c) Hall resistance of LiSn<sub>2</sub>As<sub>2</sub> single crystal with  $H//c$  axis. (d) Carrier concentrations of LiSn<sub>2</sub>As<sub>2</sub> single crystal as a function of temperature.

in the temperature range of 2-5 K. The fitting formula is [31]

$$\frac{C_P}{T} = \gamma + \beta T^2$$

$$\Theta_D = \sqrt[3]{\frac{12\pi^4 N_A r k_B}{5\beta}}$$

where  $\gamma$  is the electronic specific heat coefficient and  $\beta$  refers to the phonon specific heat coefficient. The fitted parameters are  $\gamma=2.48$  mJ mol<sup>-1</sup> K<sup>-2</sup>,  $\beta=0.89$  mJ mol<sup>-1</sup> K<sup>-2</sup> and  $\Theta_D=221$  K, which is close to the value obtained by BG model. The Debye temperature of LiSn<sub>2</sub>As<sub>2</sub> is comparable to that of NaSn<sub>2</sub>As<sub>2</sub> ( $\Theta_D=205$ K) and SrSn<sub>2</sub>P<sub>2</sub> ( $\Theta_D=237$ K). The Hall resistance and extracted carrier density of LiSn<sub>2</sub>As<sub>2</sub> are shown in Figs. 3(c) and (d). The positive slope and linear behavior of Hall resistance indicate that LiSn<sub>2</sub>As<sub>2</sub> is a single band p-type metal. The carrier density ( $n$ ) is calculated by the single band model

$$n = \frac{1}{eR_H}$$

where  $e$  is elementary charge and  $R_H$  refers to Hall coefficient. The carrier concentration of LiSn<sub>2</sub>As<sub>2</sub> is  $3.59 \times 10^{21}$

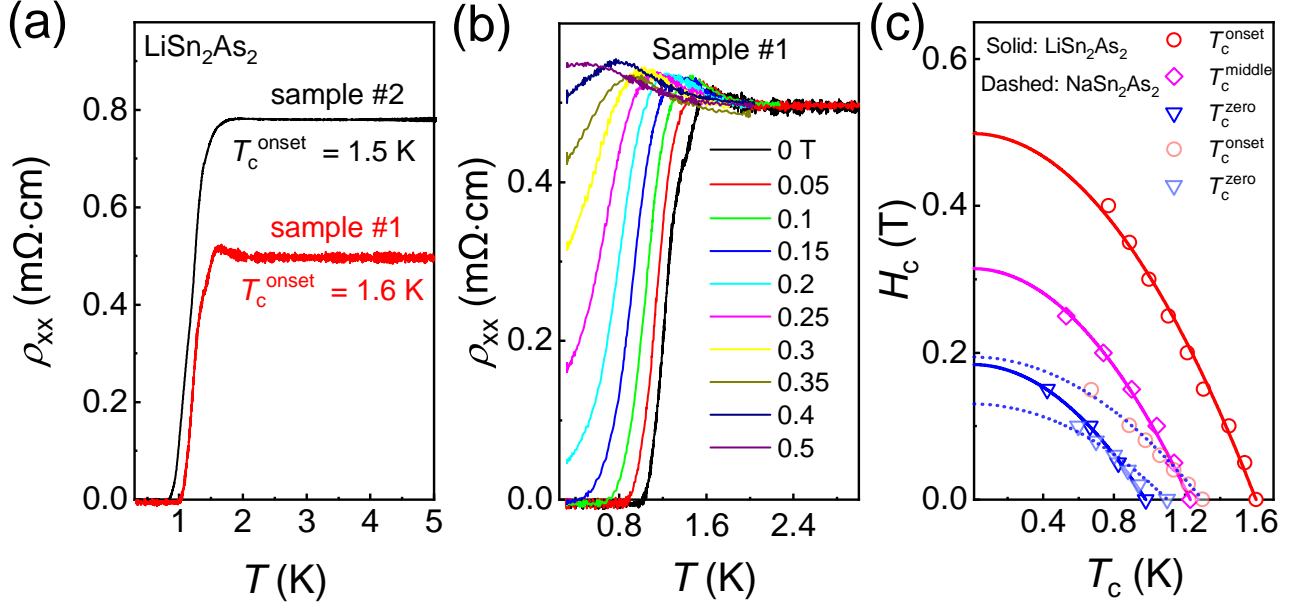


FIG. 4. (a) Low-temperature resistivity of two  $LiSn_2As_2$  single crystals from 0.3 to 5 K. (b) Low-temperature resistivity at different magnetic fields parallel to the  $c$  axis. (c) The upper critical fields ( $H_c(0)$ ) fitted by  $T_c^{onset}$ ,  $T_c^{middle}$  and  $T_c^{zero}$  with  $H//c$  axis. The dashed curve are the  $H_{c2}(T)$  of  $NaSn_2As_2$  extracted from Ref [6]

$cm^{-3}$  at 2 K and  $7.74 \times 10^{21} cm^{-3}$  at 300 K, confirming the metallic nature.

Because  $LiSn_2As_2$  and  $NaSn_2As_2$  have similar transport behavior and Debye temperatures, we are interested in learning more about  $LiSn_2As_2$ 's ultra-low temperature behavior. The resistivity of two batches of  $LiSn_2As_2$  single crystals in the temperature range of 0.3-5 K is shown in Fig. 4(a). A sharp decline in resistivity can be seen at 1.6 K, with a zero resistance reaching at 1 K. There are slight differences between two batches of  $LiSn_2As_2$  single crystals. The sample with lower residual resistance (#2) shows a lightly lower  $T_c^{onset} = 1.5$  K than that of sample #1, implying the small variation of  $T_c$  is caused by sample quality. The suppression of superconductivity at various external magnetic fields is seen in Fig. 4(b). In the presence of a magnetic field, the sample exhibits a tiny hump. This hump can also be seen in other instances, such as  $NdCeCuO$  and  $BiSrCaCuO$  [32, 33], which is generally considered to be the result of imperfection of the single crystals. Figure 4(c) shows the upper critical fields  $H_c(0)$  fitted by Ginzburg-landau equation

$$H_c(T) = H_c(0) \left[ 1 - \left( \frac{T}{T_c} \right)^2 \right]$$

The fitted  $H_c(0)$  are 0.49 T, 0.31 T and 0.18 T for  $T_c^{onset}$ ,  $T_c^{middle}$  and  $T_c^{zero}$ , respectively. We note that the acquired  $H_c(0)$  of  $LiSn_2As_2$  is much higher than that of  $NaSn_2As_2$  (0.31 T for  $T_c^{onset}$  and 0.15 T for  $T_c^{zero}$ , superimposed as dotted lines in Fig. 4(c)).

Figure 5(a) depicts the initial Brillouin zone and the

rhombohedral lattice's high symmetry route. The corresponding band structure and partial density of states (PDOS) are shown in Fig. 5(b). The bands of  $LiSn_2As_2$  are more electron doped than the band structure of  $NaSn_2As_2$  (shown as a dash curve), which is consistent with our Hall measurement. Furthermore, the Sn- $s$ , Sn- $p$ , and As- $p$  orbitals are mainly responsible for the bands around the fermi level ( $E_F$ ). The  $s$  orbital of Sn, in particular, contributes 18.3% of the total DOS at the  $E_F$ , whereas the  $s$  orbital of As lies -10 eV below the  $E_F$  (not shown here).  $LiSn_2As_2$  has two sets of Fermi surface (shown in Fig. 5(c)), the cylindrical shape one is similar to that of  $NaSn_2As_2$  [34], while the bowl shape one around Z point is attributed to the local hole-doped band characteristic of  $LiSn_2As_2$ , as the corresponding band in  $NaSn_2As_2$  is located just below the Fermi level around Z point. The stability of the acquired  $LiSn_2As_2$  is substantiated by the phonon calculations presented in Fig. 5(d). A neglectable imaginary frequency around  $\Gamma$  is caused by numerical noise.

Finally, we discuss the superconducting control parameter in the Sn-based layered Zintl phase. The volume contraction of 6.75% indicates that the iso-electron substitution of Na by Li produces an effective positive chemical pressure in  $NaSn_2As_2$ . The observation of superconductivity in  $LiSn_2As_2$  and the comparable  $T_c$  rule out chemical pressure as a key driver in  $T_c$  increase. Meanwhile,  $NaSnAs$  and  $NaSnP$  are semiconductors with narrow band gaps at about 0.31 eV and 0.63 eV respectively, and  $SrSn_2As_2$  is a semimetal [15, 35]. This semiconducting or semimetallic behavior can be explained in terms of

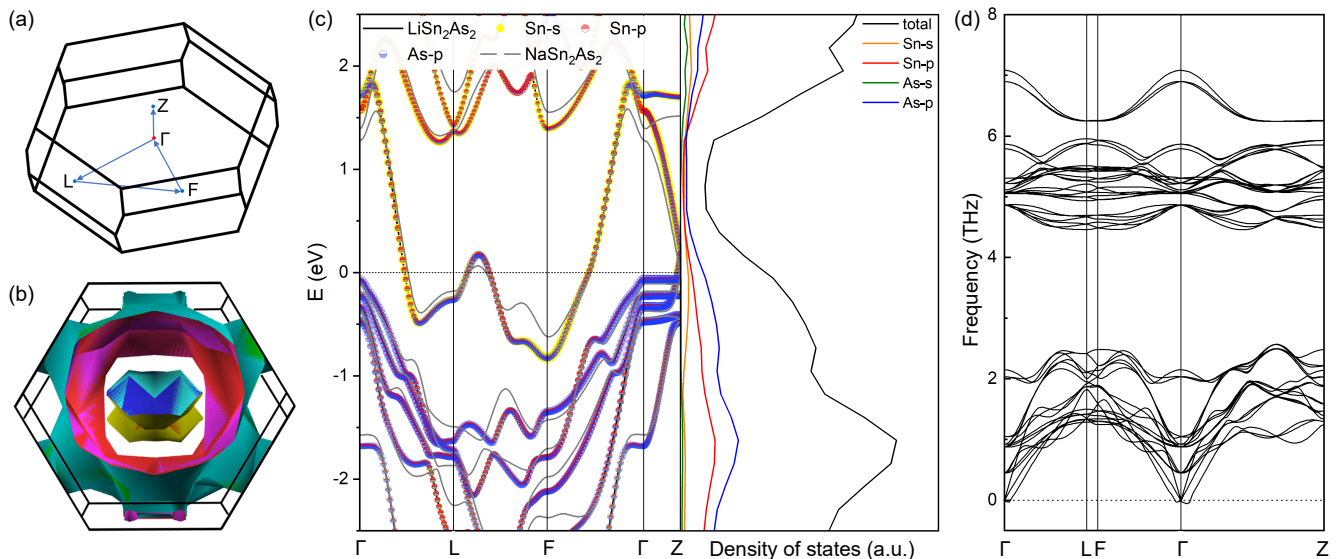


FIG. 5. (a) First Brillouin zone and the high symmetry K-path of LiSn<sub>2</sub>As<sub>2</sub>. The Fermi surface (b), band structure and partial density of states (PDOS) (c) and phonon spectrum (d) of LiSn<sub>2</sub>As<sub>2</sub>. The bands of NaSn<sub>2</sub>As<sub>2</sub> are superimposed in Fig. 5(c) as gray curve for comparison.

lone pair electrons, where the Sn-Pn tetrahedra have saturated electron pairs and the ionic bonds between the alkali metal Na and the Zintl ion SnPn do not have enough itinerant electrons, as briefly discussed in the introduction. Any hole doping can effectively tip the charge balance and boost conductivity in these double lone pair electrons, which serve as a charge reservoir. This is exactly the case of superconducting NaSn<sub>2</sub>As<sub>2</sub>, LiSn<sub>2</sub>As<sub>2</sub> and Na<sub>1-x</sub>Sn<sub>2</sub>P<sub>2</sub> by partial removal of electrons from the lone pair electrons. This observation is consistent with our Hall results of  $p$ -type charge carrier, and NaSnAs can be considered as a parent phase of the Sn-based layered Zintl phase. We infer that the (Sn<sub>2</sub>As) slab in Sn<sub>4</sub>As<sub>3</sub> provides less than one electron to the (SnAs) slab from this perspective. Because As or P have a stronger electronegativity than Sn, the charge transfer should take place on the Sn side, with the lone pair on the P side acting as a bridge of the charge transfer. Furthermore, the phonon vibration modes will be influenced by the quantity of lone pair electrons, which will affect the electron-phonon interaction and alter  $T_c$ . This could explain the slightly different  $T_c$  within NaSn<sub>2</sub>As<sub>2</sub>, Na<sub>1-x</sub>Sn<sub>2</sub>P<sub>2</sub> and LiSn<sub>2</sub>As<sub>2</sub> (the slightly electron doping effect can be observed in Fig. 5(b)). Following this route, more exciting discovery can be anticipated. In SrSn<sub>2</sub>As<sub>2</sub>, for example, superconductivity may be achieved in a 3D Dirac semimetal by removing the electrons from the lone pair electrons through selective removal of Sr or substitution.

#### IV. CONCLUSION

In conclusion, we report the crystal structure, transport properties, heat capacity and electronic structure of LiSn<sub>2</sub>As<sub>2</sub>. In the range of 2-300 K, LiSn<sub>2</sub>As<sub>2</sub> exhibits metallic behavior. The  $\Theta_D$  obtained by BG model and Debye model are 194 K and 221 K, respectively, which is closed to that of NaSn<sub>2</sub>As<sub>2</sub>. Ultra-low temperature transport measurements reveals that LiSn<sub>2</sub>As<sub>2</sub> is a superconductor with  $T_c^{onset}$  at 1.6 K. The upper critical field of LiSn<sub>2</sub>As<sub>2</sub> is  $H_c=0.49$  T, doubling that of NaSn<sub>2</sub>As<sub>2</sub>. We discovered that the amount of lone-pair electron acts as a charge reservoir and governs superconductivity by systematically analyzing the crystal structure and physical properties of Sn<sub>4</sub>As<sub>3</sub>, NaSnAs, NaSnP and ASn<sub>2</sub>Pn<sub>2</sub>. We anticipate similar phenomena can be realized in other layered Zintl phases.

#### ACKNOWLEDGMENTS

This work is financially supported by the National Key Research and Development Program of China (No. 2018YFE0202601 and 2017YFA0304700), the National Natural Science Foundation of China (No. 51922105 and 51772322), Beijing Natural Science Foundation (Grant No. Z200005).

<sup>†</sup> These authors contribute equally  
T.Y.: ying@iphy.ac.cn  
J.G.: jgguo@iphy.ac.cn

- [1] HW Kohlschutter, "Theory and research - Eduard Zintl," *NATURWISSENSCHAFTEN* **29**, 241–244 (1941).
- [2] F Laves, "Eduard Zintl's work on chemistry and structure of alloys," *NATURWISSENSCHAFTEN* **29**, 244–255 (1941).
- [3] Jialing Wang, Sabyasachi Sen, Ping Yu, Nigel D. Brown-ing, and Susan M. Kauzlarich, "Synthesis and spectroscopic characterization of P-doped  $\text{Na}_4\text{Si}_4$ ," *JOURNAL OF SOLID STATE CHEMISTRY* **183**, 2522–2527 (2010).
- [4] Frank Albert Cotton, Geoffrey Wilkinson, Carlos A Murillo, Manfred Bochmann, and Russell Grimes, *Advanced inorganic chemistry*, Vol. 6 (Wiley New York, 1988).
- [5] Hua He, Chauntae Tyson, and Svilen Bobev, "New compounds with  $[\text{As}_7]^{3-}$  clusters: Synthesis and crystal structures of the zintl phases  $\text{Cs}_2\text{NaAs}_7$ ,  $\text{Cs}_4\text{ZnAs}_{14}$  and  $\text{Cs}_4\text{CdAs}_{14}$ ," *Crystals* **1**, 87–98 (2011).
- [6] Yosuke Goto, Akira Yamada, Tatsuma D Matsuda, Yuji Aoki, and Yoshikazu Mizuguchi, "SnAs-based layered superconductor  $\text{NaSn}_2\text{As}_2$ ," *Journal of the Physical Society of Japan* **86**, 123701 (2017).
- [7] Yosuke Goto, Akira Miura, Chikako Moriyoshi, Yoshihiro Kuroiwa, Tatsuma D Matsuda, Yuji Aoki, and Yoshikazu Mizuguchi, " $\text{Na}_{1-x}\text{Sn}_2\text{P}_2$  as a new member of van der waals-type layered tin pnictide superconductors," *Scientific reports* **8**, 1–8 (2018).
- [8] Lin-Lin Wang, Adam Kaminski, Paul C. Canfield, and Duane D. Johnson, "Different topological quantum states in ternary zintl compounds:  $\text{BaCaX}$  ( $x = \text{si, ge, sn}$  and  $\text{pb}$ )," *The Journal of Physical Chemistry C* **122**, 705–713 (2018), <https://doi.org/10.1021/acs.jpcc.7b11111>.
- [9] Michael O. Ogunbunmi, Sviatoslav Baranets, Amanda B. Childs, and Svilen Bobev, "The Zintl phases  $\text{Aln}_2\text{As}_2$  ( $A = \text{Ca, Sr, Ba}$ ): new topological insulators and thermoelectric material candidates," *DALTON TRANSACTIONS* **50**, 9173–9184 (2021).
- [10] L. Y. Rong, J. Z. Ma, S. M. Nie, Z. P. Lin, Z. L. Li, B. B. Fu, L. Y. Kong, X. Z. Zhang, Y. B. Huang, H. M. Weng, T. Qian, H. Ding, and R. Z. Tai, "Electronic structure of  $\text{SrSn}_2\text{As}_2$  near the topological critical point," *SCIENTIFIC REPORTS* **7** (2017), 10.1038/s41598-017-05386-x.
- [11] Yuanfeng Xu, Zhida Song, Zhijun Wang, Hongming Weng, and Xi Dai, "Higher-order topology of the axion insulator  $\text{EuIn}_2\text{As}_2$ ," *Phys. Rev. Lett.* **122**, 256402 (2019).
- [12] Zhiping Lin, Gang Wang, Congcong Le, Huaizhou Zhao, Ning Liu, Jiangping Hu, Liwei Guo, and Xiaolong Chen, "Thermal conductivities in  $\text{nasnas}$ ,  $\text{nasnP}$ , and  $\text{NaSn}_2\text{As}_2$ : Effect of double lone-pair electrons," *Phys. Rev. B* **95**, 165201 (2017).
- [13] Shao-Fei Wang, Zhi-Gang Zhang, Bao-Tian Wang, Jun-Rong Zhang, and Fang-Wei Wang, "Zintl phase  $\text{BaAgSb}$ : Low thermal conductivity and high performance thermoelectric material in ab initio calculation," *Chinese Physics Letters* **38**, 046301 (2021).
- [14] EJ Cheng, JM Ni, FQ Meng, TP Ying, BL Pan, YY Huang, Darren C Peets, QH Zhang, and SY Li, "Nodeless superconductivity in the SnAs-based van der waals-type superconductor  $\text{NaSn}_2\text{As}_2$ ," *EPL (Euro-physics Letters)* **123**, 47004 (2018).
- [15] Q. D. Gibson, L. M. Schoop, L. Muechler, L. S. Xie, M. Hirschberger, N. P. Ong, R. Car, and R. J. Cava, "Three-dimensional dirac semimetals: Design principles and predictions of new materials," *Phys. Rev. B* **91**, 205128 (2015).
- [16] Keisuke Shinozaki, Yosuke Goto, Kazuhisa Hoshi, Ryosuke Kiyama, Naoto Nakamura, Akira Miura, Chikako Moriyoshi, Yoshihiro Kuroiwa, Hidetomo Usui, and Yoshikazu Mizuguchi, "Thermoelectric Properties of the As/P-Based Zintl Compounds  $\text{EuIn}_2\text{As}_{2-x}\text{P}_x$  ( $x=0-2$ ) and  $\text{SrSn}_2\text{As}_2$ ," *ACS APPLIED ENERGY MATERIALS* **4**, 5155–5164 (2021).
- [17] Andrew M. Ochs, Prashun Gorai, Yaxian Wang, Michael R. Scudder, Karl Koster, Curtis E. Moore, Vladan Stevanovic, Joseph P. Heremans, Wolfgang Windl, Eric S. Toberer, and Joshua E. Goldberger, "Computationally Guided Discovery of Axis-Dependent Conduction Polarity in  $\text{NaSnAs}$  Crystals," *CHEMISTRY OF MATERIALS* **33**, 946–951 (2021).
- [18] B. Eisenmann and U. Röbler, "Crystal structure of sodium phosphidostaimate(ii),  $\text{NaSnP}$ ," *Zeitschrift für Kristallographie - New Crystal Structures* **213**, 28–28 (1998).
- [19] Marc Kastner, David Adler, and H. Fritzsche, "Valence-alternation model for localized gap states in lone-pair semiconductors," *Phys. Rev. Lett.* **37**, 1504–1507 (1976).
- [20] R.J. Angel, "Dove, M.T. Structure and Dynamics an Atomic View of Materials.: Oxford (Oxford University Press), 2003. 356 pp. Price £49.95. ISBN 0-19-850677-5." *Mineralogical Magazine* **67**, 827–828 (2003), <https://pubs.geoscienceworld.org/minmag/article-pdf/67/4/827/2915715/gsmminmag.67.4.19-boo.pdf>.
- [21] Li-Dong Zhao, Shih-Han Lo, Yongsheng Zhang, Hui Sun, Gangjian Tan, Ctirad Uher, C Wolverton, Vinayak P Dravid, and Mercouri G Kanatzidis, "Ultralow thermal conductivity and high thermoelectric figure of merit in  $\text{SnSe}$  crystals," *Nature* **508**, 373–377 (2014).
- [22] Juan Rodríguez-Carvajal, "Recent advances in magnetic structure determination by neutron powder diffraction," *Physica B: Condensed Matter* **192**, 55–69 (1993).
- [23] G. Kresse and J. Furthmüller, "Efficiency of ab-initio total energy calculations for metals and semiconductors using a plane-wave basis set," *Computational Materials Science* **6**, 15–50 (1996).
- [24] John P. Perdew, Kieron Burke, and Matthias Ernzerhof, "Generalized gradient approximation made simple," *Phys. Rev. Lett.* **77**, 3865–3868 (1996).
- [25] G. Kresse and D. Joubert, "From ultrasoft pseudopotentials to the projector augmented-wave method," *Phys. Rev. B* **59**, 1758–1775 (1999).
- [26] Hendrik J. Monkhorst and James D. Pack, "Special points for brillouin-zone integrations," *Phys. Rev. B* **13**, 5188–5192 (1976).
- [27] Atsushi Togo and Isao Tanaka, "First principles phonon calculations in materials science," *Scripta Materialia* **108**, 1–5 (2015).
- [28] C A Marques, M J Neat, C M Yim, M D Watson, L C Rhodes, C Heil, K S Pervakov, V A Vlasenko, V M Pudalov, A V Muratov, T K Kim, and P Wahl, "Electronic structure and superconductivity of the non-centrosymmetric  $\text{Sn}_4\text{As}_3$ ," *New Journal of Physics* **22**, 063049 (2020).

- [29] Nevill Francis Mott, Howard Jones, H Jones, and Huw Jones, The theory of the properties of metals and alloys (Courier Dover Publications, 1958).
- [30] John Bardeen and David Pines, “Electron-phonon interaction in metals,” *Physical Review* **99**, 1140 (1955).
- [31] Michael Tinkham, Introduction to superconductivity (Courier Corporation, 2004).
- [32] M. A. Crusellas, J. Fontcuberta, and S. Piñol, “Giant resistive peak close to the superconducting transition in  $\text{La}_{2-x}\text{Ce}_x\text{CuO}_4$  single crystals,” *Phys. Rev. B* **46**, 14089–14094 (1992).
- [33] Y. M. Wan, S. E. Hebboul, D. C. Harris, and J. C. Garland, “Interlayer Josephson coupling of thermally excited vortices in  $\text{Bi}_2\text{Sr}_2\text{CaCu}_2\text{O}_{8-y}$ ,” *Phys. Rev. Lett.* **71**, 157–160 (1993).
- [34] K. Ishihara, T. Takenaka, Y. Miao, O. Tanaka, Y. Mizukami, H. Usui, K. Kuroki, M. Konczykowski, Y. Goto, Y. Mizuguchi, and T. Shibauchi, “Evidence for  $s$ -wave pairing with atomic scale disorder in the van der Waals superconductor  $\text{NaSn}_2\text{As}_2$ ,” *Phys. Rev. B* **98**, 020503 (2018).
- [35] Zhiping Lin, Gang Wang, Congcong Le, Huaizhou Zhao, Ning Liu, Jiangping Hu, Liwei Guo, and Xiaolong Chen, “Thermal conductivities in  $\text{NaSnAs}$ ,  $\text{NaSnP}$ , and  $\text{NaSn}_2\text{As}_2$ : Effect of double lone-pair electrons,” *PHYSICAL REVIEW B* **95** (2017), 10.1103/PhysRevB.95.165201.